Finite Element Investigation on the Response of Tunnel Rock-Supports in Zones Subjected To Squeezing Occurrence

Gianluca Bella[1-2], Giulio Antonucci[3], Gennaro Scognamiglio[3]
[1] University of Applied Sciences and Arts of Southern Switzerland (SUPSI)
Via Flora Ruchat-Roncati 15, Mendrisio, Switzerland, 6850
gianluca.bella@supsi.ch
[2] Pini Group SA, Department of Tunnels and Underground Works
Via Besso 7, Lugano, Switzerland, 6900
[3] Freelance, Genova, Italy, 16100

ing.antonuccigiulio@libero.it, ing_scognamiglio@libero.it

Abstract – *The minimization in the travel time for people and good is a fundamental factor in the economic progress of any nation. Achieving this objective can be realized through tunnelling, which often involves digging at significant depths. When tunnelling at high depths, the rock masses, especially if they are weak, can generate significant stress, so leading to substantial deformation during excavation operations. These large deformations around the tunnel frequently exceed the capacity of standard rock support systems, making it challenging to maintain the tunnel's stability and safety during construction. The current study deals with Finite Element analysis to investigate the stress-strain behaviour of the rock support of a deep tunnel under squeezing conditions. The rock support performances are evaluated and compared considering several fracturing conditions by means of a wide GSI range at simulating a decrease of the rock mass properties due to the proximity of tectonized zones. Different rock mass types are also studied with variations of m_i parameter and uniaxial compressive strength. The performances of the rock supports - sliding or stiff ribs - are evaluated and compared in terms of stresses and strain acting on.*

Keywords: Squeezing, tunnelling, weak conditions, sliding ribs

1. Introduction

One of the primary challenges encountered when tunneling through mountainous regions, is the squeezing behavior of some encountered rock masses, as demonstrated by over a century of experience ([1], [2]). Rock squeezing refers to significant, time-dependent deformations that occur around the tunnel, primarily associated with creep resulting from exceeding critical shear stress, and these deformations may halt during construction or continue over an extended period ([3]). According to [4], the rate of deformation, the tunnel convergence and the size of the yielding zone surrounding the tunnel are influenced by factors such as geological conditions, in-situ stresses in relation to rock mass strength, groundwater flow, pore pressure, and rock mass properties (Fig.1). The response of rock to squeezing is known to be affected by the type and structure of the rock: in squeezing zones, the rock is typically highly fractured and jointed, with low strength. Furthermore, the overburden also plays a significant role, and squeezing behavior may occur in a tunnel once a certain overburden threshold is exceeded. The literature documents various instances of squeezing occurring during the excavation of deep tunnels (Fig.2), including cases like the Saint Martin La Porte access adit ([5]) and the Monte Ceneri base Tunnel ([6]).
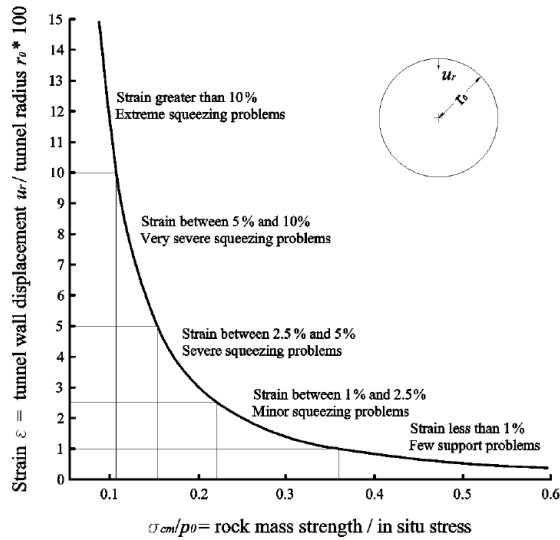
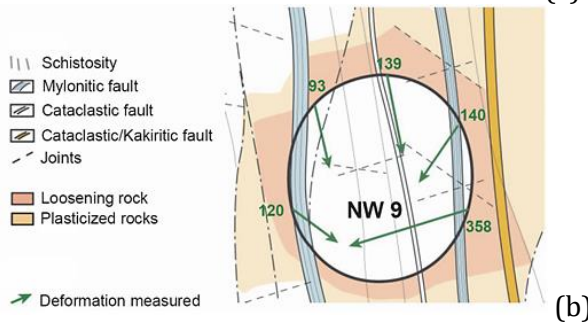Figure 1. Classification of squeezing behavior [7].

(a)

(b)

Figure 2. Relevant examples of squeezing occurrence:
a) S. Martin la Porte ([5]); b) Val Colla Line ([6]).

Squeezing is linked to the excavation technique, tunnelling sequences, and supporting methods, making the selection of rock support a crucial factor for ensuring safety and optimizing the design. Flexible rock supports permit a certain degree of displacement in the rock mass within defined limits, leading to an equilibrium between the rock mass and the support as shown by the green point in Figure 3 which is below the capacity of the rock

support. On the other hand, if the rock deformations are restricted by the adoption of rigid support systems, squeezing will cause the support to gradually accumulate load over time, with the equilibrium pressure reaching the maximum capacity, which could ultimately result in failure of the support system (red point in the same picture).
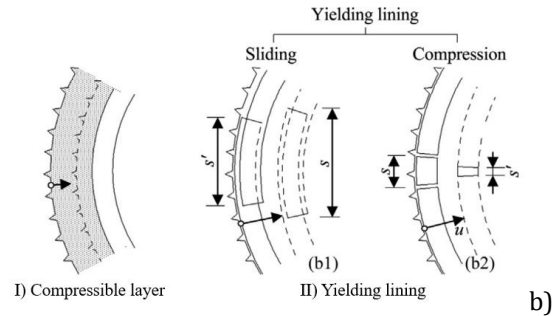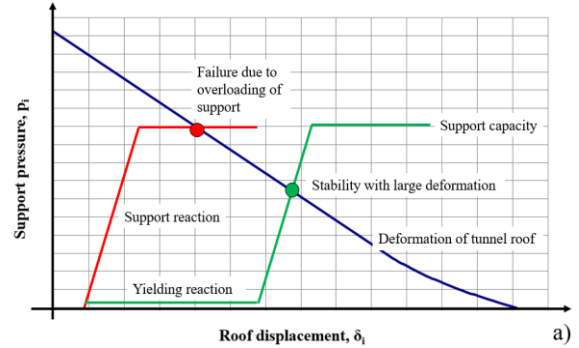

Figure 3. a) ground reaction curve (blue) and support reaction curve for stiff ribs (red) and sliding ribs (green); b) basic types of flexible support ([8])

Some details of flexible supports are given in the following picture: more information can be found in [9].
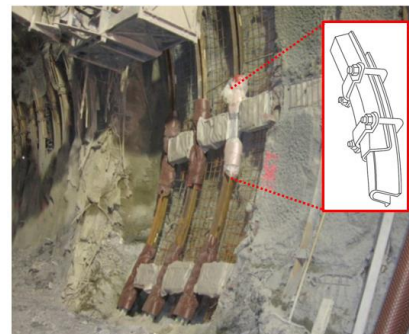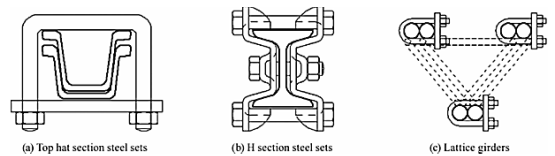

Figure 4. Top: sliding connections of top hat section steel sets, H section steel sets, and lattice girders. [9].
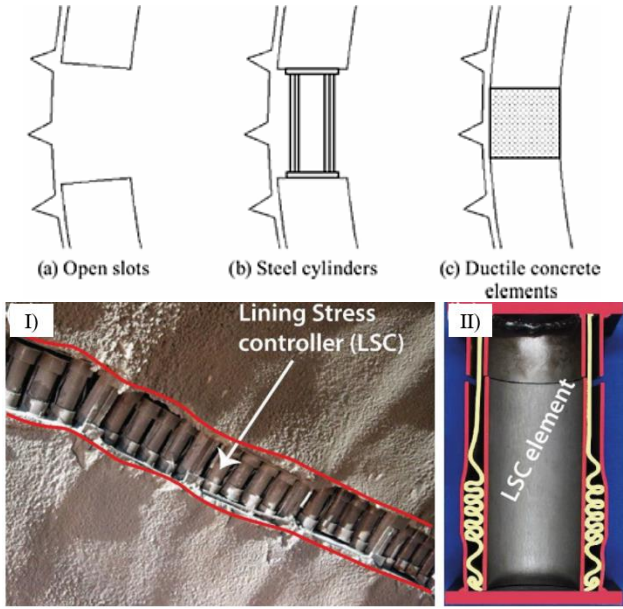
Figure 5. Shotcrete shell with open slots, steel cylinders [10], and ductile concrete elements [10] and details (modified from [9]).

In this context, the present study investigates the performance of rigid versus sliding rock supports under squeezing conditions, which are expected when tunnelling at hight depths and high stress levels. Two scenarios are considered: one involving various states of rock fracturing ('Simulation n.1') and another focused on different types of weak rock masses ('Simulation n.2') that lead to squeezing. The performances associated with using rigid or sliding ribs are evaluated and compared in terms of the strain and stresses exerted on the rock supports.

2. Numerical analysis

2.1 Finite element modelling and hypothesis

The cross-section of a circular, deep tunnel, radius R_T = 5.00m, overburden H=600m - under plane strain conditions and a constant stress state - was modelled by using the finite element software RS2v.9.0 (RocScience) as shown in Figure 6. Six noded, graded triangular meshes (total 10'000), progressively refined near significant clusters, were adopted. The shape of the mesh (triangular) has been adopted because of the simple geometry of the problem and since it allows a reduction of the computation time. Boundary conditions were defined with hinges along all sides of the model to avoid horizontal/vertical displacements, and the model dimensions (130x130m) were chosen to prevent

numerical side effects. The rock mass considered for 'Simulation n.1' consists of Shists (average value of the modulus ratio MR=550), while for the 'Simulation n.2' were analysed the following rock types: shale, phyllite, metabasics, schists, gneiss, and altered diorite (MR=150-1100). Knowledge of the uniaxial compressive strength of the intact rock and MR allows to estimate the elastic modulus of the intact rock (Eq.(1)), leading to obtaining the deformability modulus of the rock mass depending on the GSI and disturbance factor D (Eq.(2)). Moreover, quantification of the squeezing behavior requires the knowledge of the rock mass uniaxial compressive strength according to Eq.(3) proposed by [7] depending on the Hoek-Brown parameter, on the uniaxial compressive strength of intact rock, and Geological Strength Index.

$$E_i = MR \cdot UCS \tag{1}$$

$$E_d = E_i \left(0.02 + \frac{1 - D/2}{1 + e^{((60+15D-GSI)/11)}} \right) \tag{2}$$

$$\sigma_{cm} = \left(0.0034\, m_i^{0.8} \right) UCS\, [1.029 + 0.025\, e^{(-0.1m_i)}]^{GSI} \tag{3}$$

where MR is the modulus ratio, UCS is the uniaxial compressive strength of the intact rock, E_d is the deformability modulus of the rock mass, E_i is the elastic modulus of the intact rock, GSI is Geological Strength Index, D is the disturbance factor, σ_{cm} is rock mass uniaxial compressive strength, m_i is the Hoek & Brown parameter of the intact rock. An elastic-perfectly plastic Hoek-Brown failure criteria has been adopted. Dry conditions were assumed for all the analyses, while the tunnel excavation was simulated step by step (Tab.1).
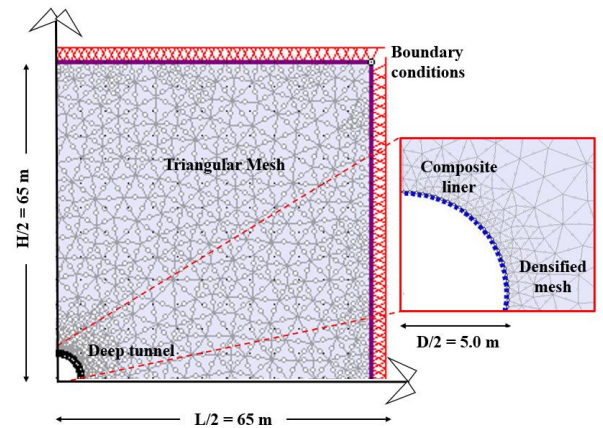

Figure 6: FE model, geometry, boundary conditions and materials.

Table 1: Finite element model steps and description.

Step	Description (X=tunnel face distance)
1	in-situ state of stress, $p_i/p_0=1.0$
2	tunnel face excavation, X=0.0m, $p_i/p_0(X)$
3	temporary lining installation, X=1.0m, $p_i/p_0(X)$
4	tunnel excavation advance, X=2.0m, $p_i/p_0(X)$
5	shotcrete curing at 5 days, X=5.0m, $p_i/p_0(X)$
6	shotcrete curing at 7 days, X=10.0m, $p_i/p_0(X)$
7	final lining installation, far from the tunnel face, distance X=20.0m, $p_i/p_0=0$

A wide range of GSI values, from 25 to 45 (analysis A → analysis E), was employed in 'Simulation n.1' to capture varying fracturing conditions. To simulate the impact of different poor-quality rock masses, ''Simulation n.2'' considered a variable range of m_i values (8-20) and uniaxial compressive strength (UCS) values (10-15MPa) across analyses A to I. In these conditions "extreme and very severe squeezing problems" are expected (Fig.1). The unit weight (γ), GSI, the Hoek & Brown m_i parameter (intact rock), UCS, Poisson's ratio (v), deformability modulus (E_d), rock mass strength (σ_{cm}), initial stress state (p_0), and the coefficient of earth pressure at rest (k_0) are detailed in Table 2 and Table 3 for ''Simulation n.1'' and ''Simulation n.2'', respectively. The rock support (primary lining) was modelled as a 'standard beam' (Tab.4). The equivalent section per meter length includes a 0.2m thick shotcrete layer and double IPN160 ribs spaced at 1.5m intervals. To represent the presence of sliding ribs in the deformable lining, four circumferential sliding slots (each 0.10m long) were incorporated, allowing for a circumferential strain of 1.2%. The final tunnel lining consists of a steel-reinforced concrete section (Tab.5).

Table 2: 'Simulation n.1'. Rock mass parameters (γ=27kN/m³, m_i=20, UCS=12MPa, v=0.30, p_0=16.2MPa, k_0=1).

Analysis →	A	B	C	D	E
GSI [-]	25	30	35	40	45
E_d [MPa]	395	537	750	1050	1480
σ_{cm} [MPa]	0.99	1.17	1.37	1.60	1.88
σ_{cm}/p_0 [-]	0.06	0.07	0.08	0.10	0.12

Table 3: 'Simulation n.2'. Rock mass parameters of shist, phyllite m_i=8, schists m_i=10, metabasics, gneiss and altered diorite m_i=20 (γ=27kN/m³, v=0.30, p_0=16.2MPa, k_0=1).

Analysis →	A	B	C	D	E
GSI [-]	40	40	40	40	40
m_i [-]	8	10	20	8	10
UCS MPa]	10	10	10	12	12
E_d [MPa]	878	878	878	1053	1053
σ_{cm} [MPa]	0.87	0.96	1.34	1.04	1.15
σ_{cm}/p_0 [-]	0.05	0.06	0.08	0.06	0.07

(part 1/2)

Analysis →	F	G	H	I
GSI [-]	40	40	40	40
m_i [-]	20	8	10	20
UCS [MPa]	12	15	15	15
E_d [MPa]	1053	1317	1317	1317
σ_{cm} [MPa]	1.60	1.30	1.44	2.00
σ_{cm}/p_0 [-]	0.10	0.08	0.09	0.12

(part 2/2)

Table 4: Equivalent rock support parameters: elastic modulus (E_{eq}), thickness (h_{eq}), area (A_{eq}), inertia (I_{eq}), Poisson's ratio (v), circumferential strain (ε_c).

	E_{eq} [MPa]	h_{eq} [m]	A_{eq} [m²]	I_{eq} [m⁴]	v [-]	ε_c [%]
Rock support type A: stiff ribs	4435	0.21	0.215	0.000826	0.20	-
Rock support type B: sliding ribs	4435	0.21	0.215	0.000826	0.20	1.2

Table 5: Final lining parameters: elastic modulus (E), spacing (s), diameter (Φ), rebar depth (d), thickness (h), area (A), inertia (I), Poisson's ratio (v), compressive strength (σ_c), tensile strength (σ_t).

	E [GPa]	s [m]	Φ [mm]	d [mm]	h [m]
Reinforcement (rebar B450C, 2 layers)	200	0.25	16	0.9	-
Concrete C20/25	30	-	-	-	1.0

(part 1/2)

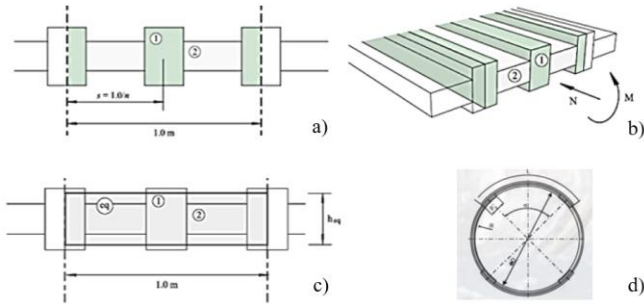|	A [mm²/m]	I [m⁴]	v [-]	σ_c [MPa]	σ_t [MPa]
Reinforcement (rebar B450C, 2 layers)	803 x 2	8.14· 10^{-5}	0.25	450	450
Concrete C20/25	-	-	0.15	25	3

(part 2/2)

Figure 7: Rock support section made of IPN ribs and shotcrete layer (a, b), equivalent section (c), and example of transversal section equipped with sliding ribs.

2.2 Design approach

FE analyses are conducted to assess the performances either for rigid ribs or sliding rock supports, following the procedure listed below:

1. An initial Convergence-Confinement two-dimensional analysis of the unsupported tunnel is performed with 10 calculation stages ($p_i/p_0 = 1.0$, $p_i/p_0 = 0.8$, $p_i/p_0 = 0.4$, $p_i/p_0 = 0.2$, $p_i/p_0 = 0.1$, $p_i/p_0 = 0.08$, $p_i/p_0 = 0.04$, $p_i/p_0 = 0.02$, $p_i/p_0 = 0.01$, and $p_i/p_0 = 0$). So, the maximum convergence (u_{max}) and the plastic radius (R_P) of the unsupported tunnel at the final stage are estimated (Fig.8);
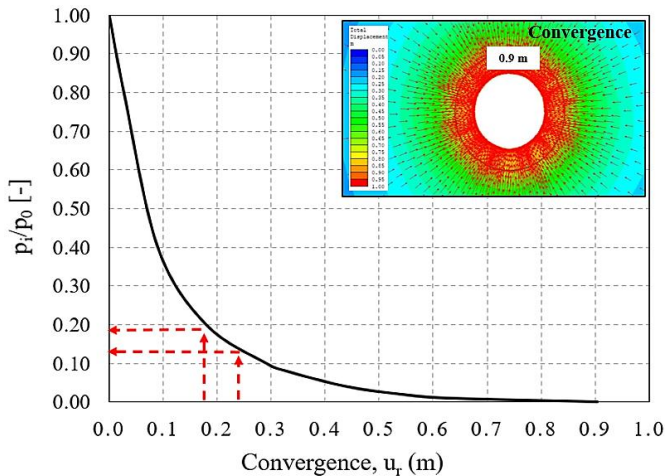

Figure 8: Evaluation of the ratio p_i/p_0, and so the relaxing factor from the ground reaction curve. Calculations for simulation n.1-analysis C are given.

2. The method outlined by [12] is used to determine the tunnel convergence (u_r) at specified distances from the tunnel face (i.e., tunnel face: X = 0m; installation of

the rock support: X = 1m), based on the ratio R_P/R_T, as shown in Fig.9;

3. Following the convergence-confinement approach ([13]), radial displacements above estimated are used to determine the ratio $p_i/p_0 = (1-\lambda)$ at both the tunnel face and the rock support installation, enabling the calculation of the relaxation factor $\lambda(X)$, as shown in Fig.8;

4. The relaxing factors allowed to perform a second series of FE analyses made of two models (Tab.1) to compare the two different rock supports.
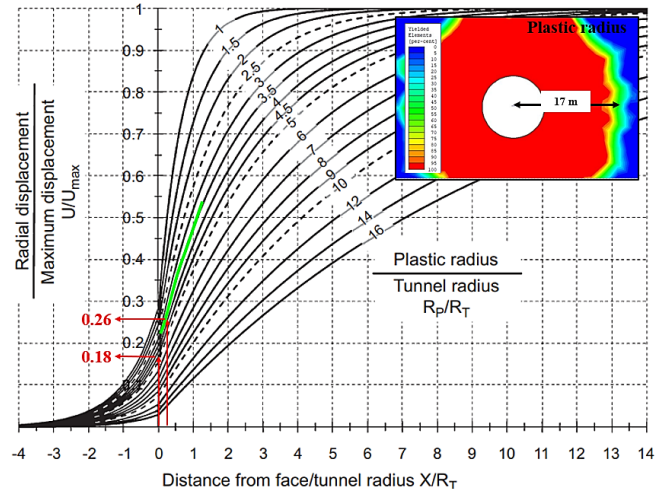

Figure 9: Solution proposed by [12] to estimate the tunnel convergence at different tunnel face distances, and plastic radius of the unsupported tunnel. Calculations for simulation n.1-analysis C are given.

3. Results

Main outcomes both for simulation n.1 and simulation n.2 are provided in the following chapters.

3.1 Simulation n.1

Table 6 presents a comparison of the FE results, considering either stiff ribs (rock support type A), or sliding ribs (rock support type B). Figure 10(top) shows the stress state MN acting on the rock support type A (represented by red symbols for stiff ribs) and type B (represented by green symbols for deformable ribs) as a function of rock mass fracturing, depicted in the interaction diagram. The safety level is also evaluated, as shown in the same Figure (middle). Due to the increased radial displacement allowed by deformable ribs, they are subjected to a lower state of stress compared to stiff ribs. Furthermore, the rock mass fracturing has little impact

on the safety level. These findings suggest that, within the considered loading conditions, tunnel shape, and stress state, deformable ribs offer a higher safety level than rock support type A. In both cases, the radial displacement increases as the quality of the rock mass decreases, whether sliding or stiff rock supports are used, as illustrated in Figure 10(bottom). A significant reduction in radial displacement with improved rock quality is more noticeable when sliding ribs are used instead of stiff ribs. The differences between stiff and sliding ribs are more evident for GSI values between 25-35 (indicating very poor rock mass quality), while for poor to medium rock mass quality, the differences become less significant.

Table 6: Simulation n.1, stiff and sliding ribs: maximum convergence at final lining installation (u), plastic radius (R_P), axial force (N_{max}), and bending moment (M_{max}).

| Ana-lysis | E_d [MPa] | GSI [-] | Rock support type A: stiff ribs | | | |
			u [m]	R_P [m]	N_{max} [MN]	M_{max} [MNm]
A	395	25	0.53	10.50	12.10	5.00
B	537	30	0.39	10.10	9.80	3.50
C	750	35	0.25	9.90	9.31	3.40
D	1050	40	0.16	8.60	9.20	3.20
E	1480	45	0.11	8.00	8.30	3.00

(part 1/2)

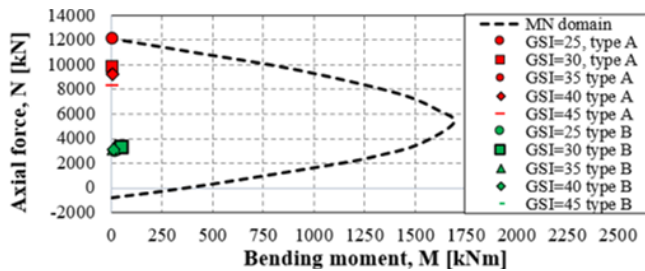| Ana-lysis | E_d [MPa] | GSI [-] | Rock support type B: sliding ribs | | | |
			u [m]	R_P [m]	N_{max} [MN]	M_{max} [MNm]
A	395	25	1.13	15.00	2.94	20.00
B	537	30	0.68	13.20	3.30	16.00
C	750	35	0.41	11.70	3.20	12.00
D	1050	40	0.25	10.40	3.10	9.00
E	1480	45	0.16	9.90	2.95	7.00

(part 2/2)

Figure 10: Top and middle: MN diagram, bottom: safety factor with GSI; bottom: maximum convergences when stiff or sliding ribs are installed.

Numerical outputs are provided with their characteristic values (FE analyses performed under GSI=35), as shown in Fig.11-14.
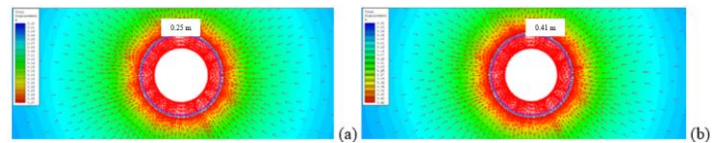

Figure 11: Simulation n.1, analysis 'C' (GSI=35) - maximum tunnel convergence in case of stiff ribs (0.25m) or sliding ribs (0.41m).
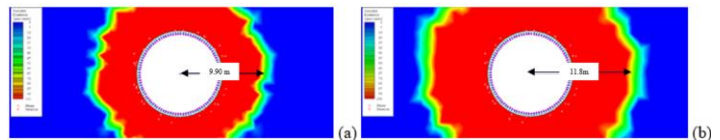

Figure 12: Simulation n.1, analysis 'C' (GSI=35) – plastic radius in case of stiff ribs (9.9m) or sliding ribs (11.8m).
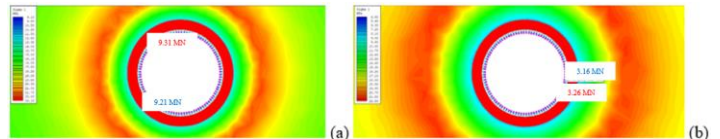

Figure 13: Simulation n.1, analysis 'C' (GSI=35) – axial force in case of stiff ribs (9.3MN) or sliding ribs (3.1MN).
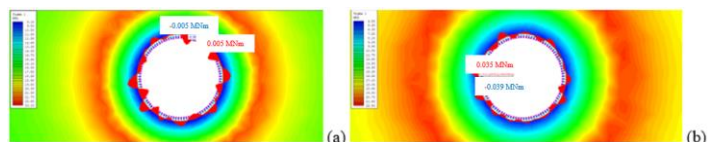

Figure 14 Simulation n.1, analysis 'C' (GSI=35) – bending moment in case of stiff (0.005MNm) ribs or sliding ribs (0.039MNm).

3.2 Simulation n.2

Table 7 provides a summary of the comparison between numerical results obtained from 'Simulation n.2', considering rock support type A (stiff ribs) and type B (sliding ribs). The comparison includes maximum convergence at the final lining installation (u), plastic radius (RP), and characteristic values of the maximum axial force (N_{max}) and maximum bending moment (M_{max}).

Table 7: Comparison between stiff and sliding ribs in terms of maximum convergence at final lining installation (u), plastic radius (RP), maximum axial force (N_{max}), maximum bending moment (M_{max}).

Ana-lysis	UCS [MPa]	m_i [-]	E_d [MPa]	Rock support type A: stiff ribs			
				u [m]	RP [m]	N_{max} [MN]	M_{max} [MNm]
A	10	8	878	0.34	14.00	14.10	4.00
B		10		0.30	12.00	12.80	5.00
C		20		0.21	9.70	9.40	5.00
D	12	8	1053	0.25	12.50	13.60	5.00
E		10		0.24	11.60	11.50	5.00
F		20		0.16	8.80	8.90	9.00
G	15	8	1317	0.19	11.60	11.15	5.00
H		10		0.16	10.40	11.00	5.00
I		20		0.12	8.40	8.00	6.00

(part 1/2)

Ana-lysis	UCS [MPa]	m_i [-]	E_d [MPa]	Rock support type B: sliding ribs			
				u [m]	RP [m]	N_{max} [MN]	M_{max} [MNm]
A	10	8	878	0.94	22.00	3.40	12.00
B		10		0.71	17.80	3.40	13.00
C		20		0.35	11.50	3.20	27.00
D	12	8	1053	0.63	19.00	3.40	10.00
E		10		0.49	16.00	3.25	10.00
F		20		0.25	10.60	3.10	28.00
G	15	8	1317	0.39	15.50	3.30	10.00
H		10		0.31	14.20	3.30	15.00
I		20		0.17	9.80	3.00	30.00

(part 2/2)

Figure 15 illustrates the effects of variations in the UCS and the m_i H-B parameter on the MN domain and the safety factor of the support. Figure 15(top) and Figure 14(middle) show the stress state acting on rock support type A (red symbols: stiff ribs) and type B (green symbols: deformable ribs), respectively. The isotropic stress state, model symmetry, and the tunnel's circular shape resulted in relatively low bending moments when compared to the axial forces acting on the rock supports. As depicted in Figure 14(bottom), variations in mi and UCS representing different poor-quality rock masses do not substantially impact the safety factor for sliding ribs

(type B, green symbols). However, for stiff ribs (type A, red symbols), there is an observed increase in the safety factor of approximately 40%. In the case of deformable ribs, the stress state is lower than that of stiff ribs due to the higher convergence allowed by the yielding system. Therefore, under the conditions considered in this study, rock support type B offers a higher safety level than stiff ribs when squeezing conditions are expected.
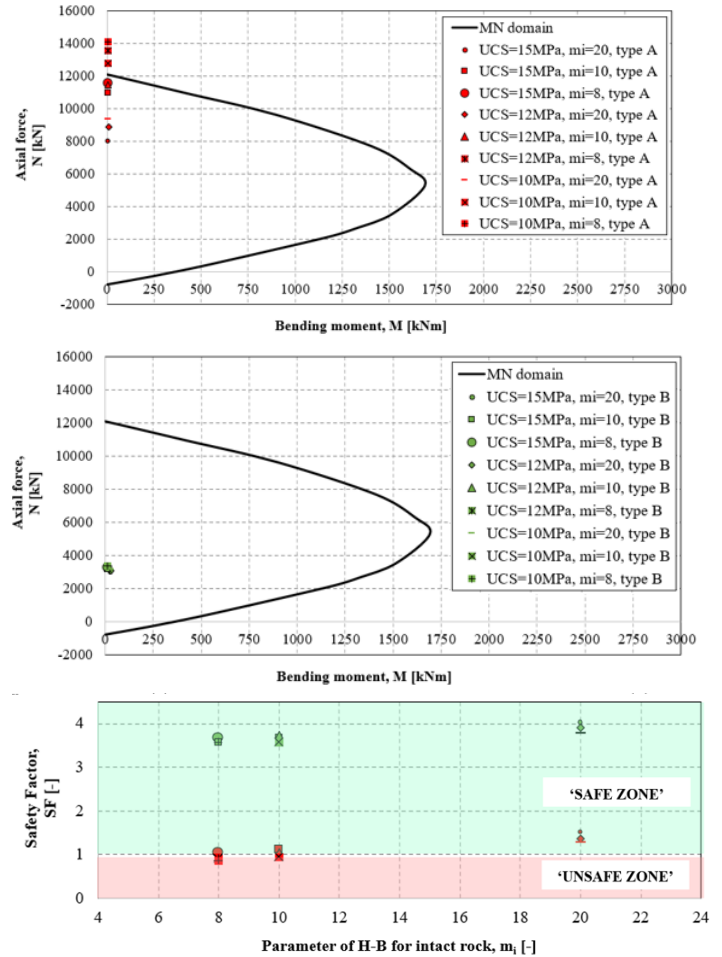

Figure 15: Interaction MN diagram in the case of stiff ribs (top), sliding ribs (middle) and safety factor with m_i and UCS (bottom).

The maximum convergences for rock support types A and B are presented in Figure 16 top and bottom, respectively, based on variations in UCS and mi. For very weak-to-poor quality rock mass (e.g., UCS=10 MPa and mi=8-15), considerable convergences ranging from 0.34 to 0.25m (for stiff ribs) or from 0.90 to 0.50 m (for sliding ribs) are observed. In cases of poor-to-medium rock mass quality (e.g., UCS=12-15MPa and mi=15-20), the

differences in convergence are minimal. As the rock mass quality improves (from UCS=12MPa-15MPa and m_i=8 to 20), the radial displacement decreases, with a more significant reduction in convergences for sliding ribs (about 2.5 times) compared to stiff ribs (1.5 times), especially when UCS remains constant, and m_i varies.
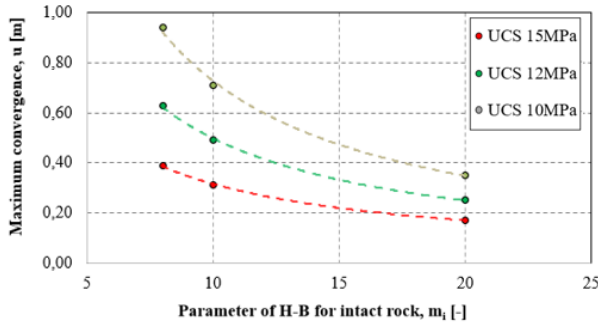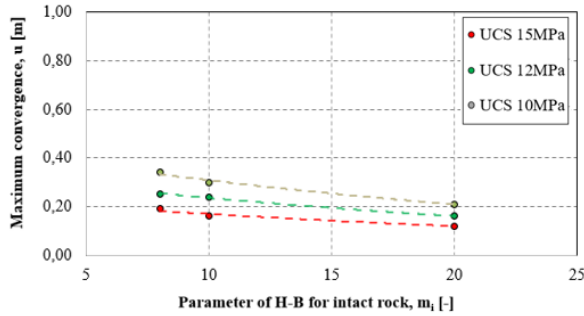

Figure 16: Maximum convergences when a) stiff ribs, or b) sliding ribs are applied.

Numerical results are also presented for analyses conducted with GSI=40, UCS=12MPa, and m_i=10, as illustrated in Figures 17-20.
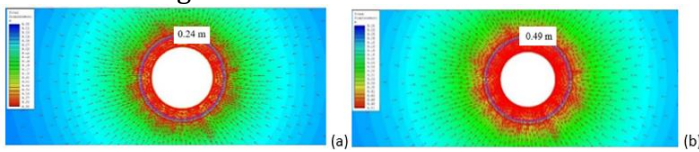

Figure 17: Simulation n.2, analysis 'E' (GSI=40, UCS=12, m_i=10) - maximum tunnel convergence in case of stiff ribs (0.24m) or sliding ribs (0.49m).
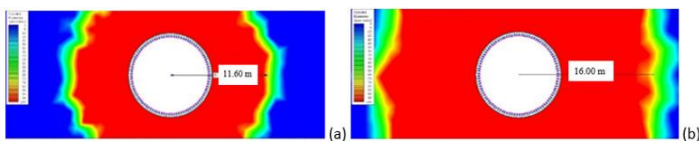

Figure 18: Simulation n.2, analysis 'E' (GSI=40, UCS=12, m_i=10) - plastic radius in case of stiff ribs (11.6m) or sliding ribs (16.0m).
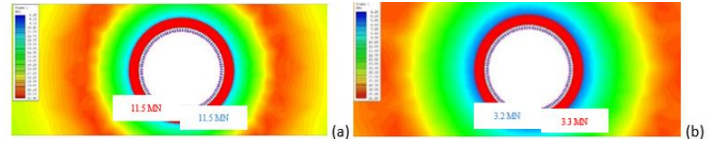

Figure 19: Simulation n.2, analysis 'E' (GSI=40, UCS=12, m_i=10) - axial force in case of stiff ribs (11.5MN) or sliding ribs (3.3MN).
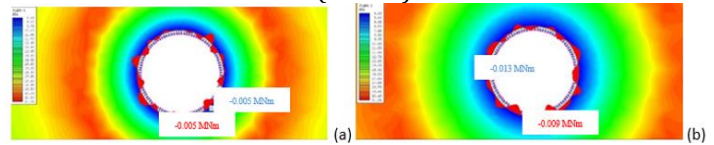

Figure 20 Simulation n.2, analysis 'E' (GSI=40, UCS=12, m_i=10) - bending moment in case of stiff (0.005MNm) ribs or sliding ribs (0.013MNm).

4. Conclusion

This study provided an insight into the stress-strain behavior of a deep, circular tunnel cut through a weak rock mass. It also explores the safety levels associated with various types of rock supports and rock mass characteristics, based on finite element analysis. This helps to draw some preliminary suggestions regarding the choice between yielding or rigid rock supports in scenarios involving squeezing behavior. According to 'Simulation n.1', the fracturing of the rock mass does not appear to significantly influence the safety level, while deformable supports are found to offer better safety compared to rigid ones. Additionally, 'Simulation 2' reveals that yielding supports are more responsive when dealing with weak or poor-quality rock masses. This is because sliding elements allow for larger convergences and result in a lower stress state, thus improving the safety factor. In contrast, the safety criteria are not met with stiff ribs in weak-poor quality rock. However, for rock masses of medium quality, both stiff and sliding ribs maintain an acceptable safety factor, which increases notably as the geo-mechanical parameters improve.

The above results and so effectiveness in adopting yielding supports when squeezing behavior was expected, have been confirmed by recent tunnelling experiences given by literature ([6]).

Additional investigations could be carried out by employing more advanced constitutive models that incorporate long-term behavior, such as creep, or by examining the tunnel excavation process under an anisotropic stress state. These enhanced models would offer a more comprehensive understanding of the material's response over extended periods and in

complex stress conditions, ultimately leading to more accurate predictions of the tunnel's stability and performance throughout its construction and operational lifespan.

References

[1] G. Antonucci, G. Bella, G. and Scognamiglio, "Numerical Analysis of Tunnel Supports in Weak Ground Conditions and High Stress Levels", in Proceeding of the *5th International Conference on Civil Engineering Fundamentals and Applications (ICCEFA 2024)*, Lisbon, Portugal, vol. 01, pp, 1-8, 2024.

[2] G. Scognamiglio, G. Antonucci, and G. Bella, "On the stress-strain response of deep tunnel in squeezing conditions: numerical analysis for the design of rock supports", in Proceeding of the *10th International Conference on Geotechnical Research and Engineering (ICGRE 2025)*, Barcelona, Spain, vol. 01, pp. 1-8, 2025.

[3] G. Barla, "Squeezing rocks in tunnels", *ISRM News Journal*, 3/4, pp. 44-49, 1995.

[4] W. Steiner, "Tunnelling in squeezing rocks: case histories", *Rock Mech. and Rock Eng.*, vol. 29, pp. 211-246, 1996.

[5] G. Barla, "Innovative tunneling construction method to cope with squeezing at the Saint Martin La Porte access adit (Lyon-Turin Base Tunnel)", in Proceedings of the *Eurock 2009 Rock Engineering in Difficult Ground Conditions*, Dubrovnik, Croatia, vol. 01, pp. 1-10, 2009.

[6] D. Merlini, D. Stocker, M. Falanesca and R. Schuerch, "The Ceneri Base Tunnel: Construction experience with the Southern Portion of the Flat Railway Line Crossing the Swiss Alps", *Engineering*, vol. 1, no. 02, pp. 235-248, 2018.

[7] E. Hoek and P. Marinos "Predicting tunnel squeezing problems in weak heterogeneous rock masses", *Tunnels and Tunnelling International*, vol. 32, no. 11, pp. 45-51, 2000.

[8] K. Kovári, C. Amstad and G. Anagnostou, "Design / Construction methods Tunnelling in swelling rocks", in Proceeding of the *29th U.S. Symposium Key Questions in Rock Mechanics,* Minnesota, pp. 17-32, 1988.

[9] M. Ghorbania, K. Shahriara, M. Sharifzadehb and R. Masoudic, "A critical review on the developments of rock support systems in high stress ground conditions", *International Journal of Mining Science and Technology*, vol. 30, pp. 555–572, 2020.

[10] W. Schubert, "Dealing with Squeezing Conditions in Alpine Tunnels", *Rock Mech Rock Eng*, vol. 29, no. 03, pp.145–53, 1996.

[11] K. Kovári, "Method and device for stabilizing a cavity excavated in underground construction". US Patent 20050191138, 2005.

[12] N. Vlachopoulos and M.S. Diederichs, "Improved longitudinal displacement profiles for convergence confinement analysis of deep tunnels", *Rock Mechanics and Rock Engineering*, vol. 42, no. 02, pp. 131-146, 2009.

[13] M. Panet and A. Guenot, "Analysis of convergence behind the face of a tunnel", in Proceeding of the *International Symposium Tunnelling, (IST'82), The Institution of Mining and Metallurgy*, London, pp. 197-204, 1982.